Paper AAS 03-124

Integrated Power and Attitude Control for a Spacecraft with Flywheels and Control Moment Gyroscopes

Carlos M. Roithmayr
NASA Langley Research Center, Hampton, Virginia

Christopher D. Karlgaard, Renjith R. Kumar, and David M. Bose
Analytical Mechanics Associates Inc., Hampton, Virginia

13th AAS/AIAA Space Flight Mechanics Meeting

Ponce, Puerto Rico 9–13 February 2003

AAS Publications Office, P.O. Box 28130, San Diego, CA 92198

AAS 03-124

INTEGRATED POWER AND ATTITUDE CONTROL FOR A SPACECRAFT WITH FLYWHEELS AND CONTROL MOMENT GYROSCOPES

Carlos M. Roithmayr*
NASA Langley Research Center
Hampton, VA 23681-2199

Christopher D. Karlgaard, Renjith R. Kumar, and David M. Bose
Analytical Mechanics Associates Inc.†
Hampton, VA, 23666

A law is designed for simultaneous control of the orientation of an Earth-pointing spacecraft, the energy stored by counter-rotating flywheels, and the angular momentum of the flywheels and control moment gyroscopes used together as an integrated set of actuators for attitude control. General, nonlinear equations of motion are presented in vector-dyadic form, and used to obtain approximate expressions which are then linearized in preparation for design of control laws that include feedback of flywheel kinetic energy error as a means of compensating for damping exerted by rotor bearings. Two flywheel "steering laws" are developed such that torque commanded by an attitude control law is applied while energy is stored or discharged at the required rate. Using the International Space Station as an example, numerical simulations are performed to demonstrate control about a torque equilibrium attitude, and illustrate the benefits of kinetic energy error feedback.

INTRODUCTION

Flywheels offer great promise for reducing the mass and extending the life of spacecraft; they store more energy per unit of mass and last significantly longer than chemical batteries. Moreover, flywheels can simultaneously store energy and exert torque on a spacecraft, making it possible for one system of flywheels to replace two separate systems typically used for energy storage and attitude control. When the mass of the two conventional systems is taken into account, the specific energy of flywheel systems is expected to be 5 to 10 times greater, according to Ref. [1]. The attitude control system typically represents 11% of the mass of a spacecraft, and batteries make up 6% of the mass; replacing 17% of a spacecraft's mass with a flywheel system whose mass is 1.7% would lead to a 15%

*Mail Stop 328, E-Mail: c.m.roithmayr@larc.nasa.gov, Tel: (757) 864 6778
†303 Butler Farm Road, Suite 104 A, E-Mail: {karlgaard, renji, dmbose}@ama-inc.com, Tel: (757) 865 0944

reduction in total spacecraft mass. Secondary benefits occur as well; since flywheels have higher system level efficiencies than batteries, a reduction in solar array size and mass becomes possible, and reboost propellant can be reduced because the smaller arrays produce less drag. Flywheel systems are expected to last 15 years (Ref. [1]) or more whereas typical batteries last only 5 years. The greatest advantage of flywheels over batteries accrues in low earth orbit where eclipse happens more frequently and for larger fractions of an orbit than in higher orbits; repeated charge and discharge cycles, and high depth of discharge significantly degrade batteries over time.

Consideration was recently given (Ref. [2]) to replacing the International Space Station (ISS) batteries with a Flywheel Energy Storage System (FESS); hence, there naturally arose the thought of using the flywheels to assist the ISS Control Moment Gyroscopes (CMGs) in controlling attitude. A numerical investigation of the merits of this idea requires a feedback control law designed for CMGs and flywheels used together as an integrated set of effectors. The current CMG control law described in Refs. [3] and [4] minimizes a cost function involving spacecraft attitude and angular speed, and CMG angular momentum. A CMG steering law, such as the one developed by Kennel in Ref. [5], determines the speeds of the two gimbals (in which each constant speed CMG rotor is mounted) needed to produce the torque requested by the control law. As a natural extension of the present approach, we seek a new control law derived from a cost function that includes flywheel angular momentum in addition to the aforementioned quantities. Also needed is a "flywheel steering law," a counterpart to the CMG steering law that will determine the motor-generator torque to be applied to each member of a counter-rotating flywheel pair such that rotational kinetic energy is stored or discharged in the required manner, and the net torque requested by the control law is produced simultaneously.

A review of the literature does not reveal any existing three-axis control laws for earth-pointing spacecraft using flywheels and CMGs together, or even flywheels alone, where attitude control, momentum management, and power management are addressed in a unified way. In Ref. [6], Notti, Cormack, and Klein give a sketch of a control law and an energy distribution law; however, this work is not applicable primarily because each flywheel rotor is assumed to be supported by two gimbals and the ISS FESS did not contain any gimbals. In addition, the control law lacks flywheel angular momentum as a feedback parameter. Recent work on control laws for integrated power and attitude control systems deals either with sets of four or more flywheels whose spin axes are non-collinear (Refs. [7]–[9]), or with sets of variable-speed, single-gimbal control moment gyroscopes (Refs. [10]–[12]); neither of these types of configurations are directly applicable to the counter-rotating flywheel pair arrangement of the FESS. Varatharajoo and Fasoulas develop control laws in Ref. [13] for a spacecraft using a counter-rotating flywheel configuration; however, they only consider a pitch-axis controller.

Hall's control law, proposed in Ref. [7], is an open-loop scheme (rather than a feedback law) for performing large-angle attitude maneuvers. It does not account for gravitational and aerodynamic torques which have a significant effect on the motion of ISS, and therefore can not be used for maintaining torque equilibrium attitude, the primary job of the CMGs. Hall introduces a flywheel steering law based on a matrix pseudo-inverse; it is applied in each of Refs. [8]–[12]. Tsiotras, Shen, and Hall employ Lyapunov stability theory in Ref. [8] to develop a feedback control law which performs well in simulations involving disturbance torques; however, flywheel momentum is managed by expenditure of propellant. Costic et al. develop in Ref. [9] a nonlinear controller which includes an adaptive scheme for estimating the mass distribution of the spacecraft, but they do not address momentum management.

In Ref. [10], Fausz and Richie extend the work of Hall to a nonlinear feedback controller applicable to a set of variable-speed, single-gimbal control moment gyroscopes. Together with Tsiotras, they continue their discussion in Ref. [11] and present simulation results, but momentum management is not addressed in either of the two papers. Yoon and Tsiotras develop an adaptive nonlinear control law in Ref. [12], and incorporate wheel-speed equalization to reduce the possibility of singularities

and keep the wheel speeds within acceptable limits. Numerical simulation results show that attitude and power profiles can be tracked even when the spacecraft inertia properties are unknown. Of all the papers mentioned heretofore, Ref. [12] is the only one in which attitude control, momentum management, and power management for flywheels is considered in an integrated fashion.

It is important to note that Refs. [7]–[13] fail to take into account damping torque exerted by the spacecraft and a flywheel rotor on each other; in practice, this will cause the actual rotational kinetic energy possessed by the flywheels to differ from the required amount. None of these works include any feedback of errors in flywheel power or kinetic energy, something which must be done under realistic conditions.

In what follows we present equations of motion to be used in numerical simulations and in control law design, develop two flywheel steering laws, design an algorithm for managing momentum and maintaining torque equilibrium attitude, and present simulation results showing the performance of the control law as well as the benefits of flywheel kinetic energy error feedback.

EQUATIONS OF MOTION FOR SPACECRAFT WITH FLYWHEELS AND CMGS

Dynamical Equations

The system of interest, S, is composed of a rigid body B moving in an inertial or Newtonian reference frame N, and several rigid axisymmetric rotors $R_1, \ldots, R_\rho$ whose mass centers are fixed in B. A subset of the rotors $R_1, \ldots, R_\mathcal{F}$ have spin axes fixed in B so that these rotors represent non-gimballed flywheels or reaction wheels. Each of the remaining rotors $R_{\mathcal{F}+1}, \ldots, R_\rho$ are attached to B with one or more massless gimbals which permit the direction of the spin axis to change relative to B; these rotors thus represent a number of CMGs, $\mathcal{C} = \rho - \mathcal{F}$. (The latter subset could contain gimballed flywheel rotors as well as CMGs, but we concern ourselves in this work only with non-gimballed flywheels.) This system is illustrated in Fig. 1, with rotors $R_2, \ldots, R_{\rho-1}$ omitted for the sake of clarity.

The equations of motion are derived using Kane's method (Eqs. (6.1.2), Ref. [14])

$$F_r + F_r^\star = 0 \qquad (r = 1, \ldots, n) \tag{1}$$

where F_r are generalized active forces for S in N, $F_r^\star$ are generalized inertia forces for S in N, and n is the number of degrees of freedom of S in N.

The system S is holonomic and therefore a complete description of the motion of S in N requires n generalized speeds $u_1, \ldots, u_n$, conveniently chosen as follows.

$$^N\boldsymbol{\omega}^B = u_1\hat{\mathbf{b}}_1 + u_2\hat{\mathbf{b}}_2 + u_3\hat{\mathbf{b}}_3 \tag{2}$$

where $^N\boldsymbol{\omega}^B$ is the angular velocity of B in N, and $\hat{\mathbf{b}}_1$, $\hat{\mathbf{b}}_2$, and $\hat{\mathbf{b}}_3$ are a set of mutually orthogonal, right-handed unit vectors fixed in B.

We introduce unit vectors $\hat{\boldsymbol{\beta}}_i$ fixed in B such that they are each parallel to the spin axis of a flywheel rotor R_i, and therefore to the angular velocity $^B\boldsymbol{\omega}^{R_i}$ of R_i in B. Generalized speeds $u_4, \ldots, u_{\mathcal{F}+3}$ associated with the flywheels can then be used to write the angular velocities as

$$^B\boldsymbol{\omega}^{R_i} = u_{i+3}\,\hat{\boldsymbol{\beta}}_i \qquad (i = 1, \ldots, \mathcal{F}) \tag{3}$$

The inner gimbal of each CMG is fastened to B with a revolute joint in a single-gimbal configuration, whereas a double-gimbal CMG has the inner gimbal attached with a revolute joint to an outer gimbal, which is in turn mounted in B with a second revolute joint. The axis of each revolute

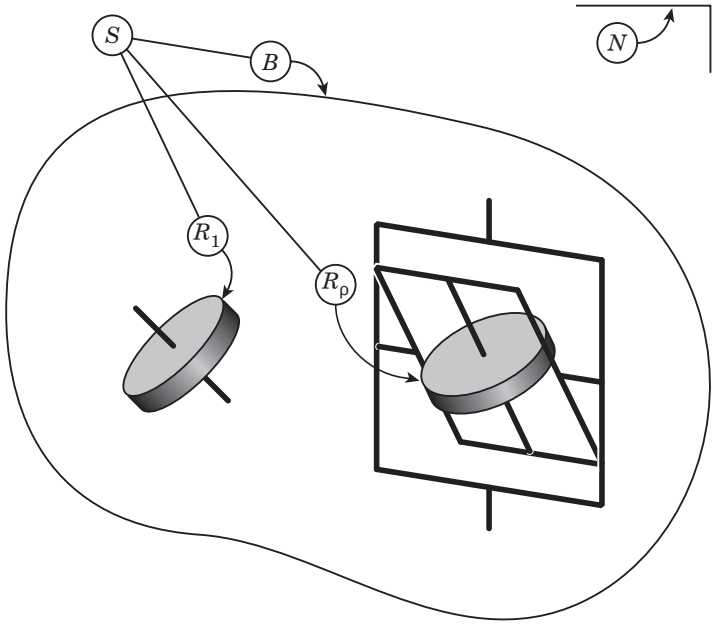

Figure 1: Spacecraft with Flywheel and CMG

joint is assumed to pass through the mass center of the rotor, which is thus fixed in B. In order to maintain generality with regard to the number of CMG rotors and gimbals, the angular velocities ${}^{B}\boldsymbol{\omega}^{R_{\mathcal{F}+1}}, \ldots, {}^{B}\boldsymbol{\omega}^{R_{\rho}}$ of the rotors relative to B are not written explicitly, but they must be functions of the generalized speeds $u_{\mathcal{F}+4}, \ldots, u_{n-3}$, where one generalized speed is required for every gimbal.

The final three generalized speeds are associated with the velocity of the mass center $S^{\star}$ of S in N,

$$ {}^{N}\mathbf{v}^{S^{\star}} = u_{n-2}\hat{\mathbf{n}}_1 + u_{n-1}\hat{\mathbf{n}}_2 + u_n\hat{\mathbf{n}}_3 \tag{4} $$

where $\hat{\mathbf{n}}_1$, $\hat{\mathbf{n}}_2$, and $\hat{\mathbf{n}}_3$ are a set of mutually orthogonal, right-handed unit vectors fixed in N.

Let σ be the set of forces exerted on S *except* those exerted by B and R_i on each other ($i = 1, \ldots, \rho$). The forces in σ acting on $B, R_1, \ldots, R_\rho$ are equivalent to single forces $\mathbf{F}_B, \mathbf{F}_1, \ldots, \mathbf{F}_\rho$ applied at the mass centers $B^{\star}, R_1^{\star}, \ldots, R_\rho^{\star}$ of bodies $B, R_1, \ldots, R_\rho$, respectively, together with couples whose torques are $\mathbf{M}_B, \mathbf{M}_1, \ldots, \mathbf{M}_\rho$.

To account for the forces exerted by B on R_i, we regard them as equivalent to a single force $\mathbf{F}^{B/R_i}$ applied at $R_i^{\star}$, together with a couple whose torque is $\mathbf{M}^{B/R_i}$. Since $R_i^{\star}$ is fixed in B, $\mathbf{F}^{B/R_i}$ contributes nothing to F_r ($i = 1, \ldots, \rho; r = 1, \ldots, n$).

The generalized active forces for S in N are obtained by application of Eq. (4.6.1) of Ref. [14], and are given by

$$ F_r = {}^{N}\mathbf{v}_r^{S^{\star}} \cdot \mathbf{F} + {}^{N}\boldsymbol{\omega}_r^{B} \cdot \mathbf{M} + \sum_{i=1}^{\rho} {}^{B}\boldsymbol{\omega}_r^{R_i} \cdot \left(\mathbf{M}_i + \mathbf{M}^{B/R_i}\right) \qquad (r = 1, \ldots, n) \tag{5} $$

where ${}^{N}\mathbf{v}_r^{S^{\star}}$ is known as the rth partial velocity of $S^{\star}$ in N, ${}^{N}\boldsymbol{\omega}_r^{B}$ is the rth partial angular velocity of B in N, and so forth. The vector $\mathbf{F}$ is the resultant of the forces in σ acting on S, $\mathbf{F} = \mathbf{F}_B + \sum_{i=1}^{\rho} \mathbf{F}_i$, and $\mathbf{M}$ is the moment of σ about $S^{\star}$, given by $\mathbf{M} = \mathbf{M}_B + \mathbf{r}^{S^{\star}B^{\star}} \times \mathbf{F}_B + \sum_{i=1}^{\rho} \left(\mathbf{M}_i + \mathbf{r}^{S^{\star}R_i^{\star}} \times \mathbf{F}_i\right)$, where $\mathbf{r}^{S^{\star}B^{\star}}$ is the position vector from $S^{\star}$ to $B^{\star}$, etc.

The generalized inertia forces for S in N are formed according to Eqs. (4.11.5)–(4.11.7) of Ref. [14], and are given by

$$
\begin{aligned}
F_r^\star = &- {}^N\mathbf{v}_r^{S^\star} \cdot m_S \, {}^N\mathbf{a}^{S^\star} - {}^N\boldsymbol{\omega}_r^B \cdot \Bigg[\underline{\mathbf{I}}^{S/S^\star} \cdot {}^N\boldsymbol{\alpha}^B + {}^N\boldsymbol{\omega}^B \times \underline{\mathbf{I}}^{S/S^\star} \cdot {}^N\boldsymbol{\omega}^B \\
&+ \sum_{i=1}^{\rho} \left(\frac{{}^B d}{dt} \, {}^B\mathbf{H}^{R_i/R_i^\star} + {}^N\boldsymbol{\omega}^B \times {}^B\mathbf{H}^{R_i/R_i^\star} \right) \\
&+ \sum_{i=\mathcal{F}+1}^{\rho} \left({}^B\boldsymbol{\omega}^{R_i} \times \underline{\mathbf{I}}^{R_i/R_i^\star} - \underline{\mathbf{I}}^{R_i/R_i^\star} \times {}^B\boldsymbol{\omega}^{R_i} \right) \cdot {}^N\boldsymbol{\omega}^B \Bigg] \\
&- \sum_{i=1}^{\rho} {}^B\boldsymbol{\omega}_r^{R_i} \cdot \frac{{}^N d}{dt} \, {}^N\mathbf{H}^{R_i/R_i^\star} \qquad (r = 1, \ldots, n)
\end{aligned} \tag{6}
$$

where m_S is the mass of system S, ${}^N\mathbf{a}^{S^\star}$ is the acceleration of $S^\star$ in N, $\underline{\mathbf{I}}^{S/S^\star}$ is the inertia dyadic of S for $S^\star$, ${}^N\boldsymbol{\alpha}^B$ is the angular acceleration of B in N, $\underline{\mathbf{I}}^{R_i/R_i^\star}$ is the inertia dyadic of R_i for $R_i^\star$, and the central angular momenta of R_i in B, and in N, are denoted respectively by ${}^B\mathbf{H}^{R_i/R_i^\star}$, and ${}^N\mathbf{H}^{R_i/R_i^\star}$. Differentiation with respect to time in B, and in N, are indicated respectively by ${}^Bd/dt$ and ${}^Nd/dt$.

According to Eqs. (1) the generalized inertia forces from Eqs. (6) are added to the generalized active forces from Eqs. (5) to yield vector-dyadic equations of motion for a spacecraft containing flywheels and CMGs

$$
\begin{aligned}
&{}^N\mathbf{v}_r^{S^\star} \cdot \left(\mathbf{F} - m_S \, {}^N\mathbf{a}^{S^\star} \right) \\
&+ {}^N\boldsymbol{\omega}_r^B \cdot \Bigg\{ \mathbf{M} - \Bigg[\underline{\mathbf{I}}^{S/S^\star} \cdot {}^N\boldsymbol{\alpha}^B + {}^N\boldsymbol{\omega}^B \times \underline{\mathbf{I}}^{S/S^\star} \cdot {}^N\boldsymbol{\omega}^B \\
&+ \sum_{i=1}^{\rho} \left(\frac{{}^B d}{dt} \, {}^B\mathbf{H}^{R_i/R_i^\star} + {}^N\boldsymbol{\omega}^B \times {}^B\mathbf{H}^{R_i/R_i^\star} \right) \\
&+ \sum_{i=\mathcal{F}+1}^{\rho} \left({}^B\boldsymbol{\omega}^{R_i} \times \underline{\mathbf{I}}^{R_i/R_i^\star} - \underline{\mathbf{I}}^{R_i/R_i^\star} \times {}^B\boldsymbol{\omega}^{R_i} \right) \cdot {}^N\boldsymbol{\omega}^B \Bigg] \Bigg\} \\
&+ \sum_{i=1}^{\rho} {}^B\boldsymbol{\omega}_r^{R_i} \cdot \left(\mathbf{M}_i + \mathbf{M}^{B/R_i} - \frac{{}^N d}{dt} \, {}^N\mathbf{H}^{R_i/R_i^\star} \right) = 0 \qquad (r = 1, \ldots, n)
\end{aligned} \tag{7}
$$

Eqs. (7) are completely general with regard to the number and orientation of flywheel rotors, and the number of CMG rotors and gimbals. In this form, they are applicable to variable-speed CMGs. These equations of motion, and the expression for generalized inertia forces, can be compared briefly to previous work.

Reference [15] is concerned with gyrostats and relevant equations that can be dealt with easily by an analyst, and quickly by a computer. Expressions for generalized inertia forces are presented separately for a gyrostat containing a single cylindrical rotor, and for one containing a single spherical rotor; an underlying general relationship (C65) developed in Appendix C can be shown to give rise to Eqs. (6) presented here, when no CMGs are present ($\mathcal{C} = 0$, thus $\rho = \mathcal{F}$). The term in the second line of Eqs. (C65) accounts for but a single rotor, although additional rotors can be handled straightforwardly by adding a sum of similar terms. The correspondence between Eqs. (C65) and our (6) is shown by appealing to Eqs. (24), (C61), (C35), (C24), (3), and (C34) of Ref. [15], and replacing their labels G, B, and A for the gyrostat, rotor, and carrier respectively with our S, R_i, and B. The use of the system mass and inertia scalars, together with the moment of inertia for the

axis of symmetry of each rotor, is shown in Ref. [15] to lead to greater efficiency than use of mass properties of individual bodies in a gyrostat; this advantage happens to accrue to Eqs. (6) and (7) developed here.

Rheinfurth and Carroll present in Ref. [16] vector-dyadic equations of motion (27) for a spacecraft composed of a rigid carrier and a rigid appendage whose mass center is fixed in the carrier. Additional appendages are accounted for easily by forming a sum, as they do in Eq. (16), but the resulting vector-dyadic expression will give rise to only three scalar equations. It is pointed out near the bottom of p. 6 that a CMG can be regarded as an appendage; however, the motion of every appendage relative to the carrier must be prescribed if the three relationships are to serve as dynamical equations governing the motion of the carrier. Reference [16] does not contain counterparts to the $n-6$ of our Eqs. (7) that govern the motion of the rotors, or to the three equations governing the translational motion of the system. It can be shown rather easily that Rheinfurth and Carroll's Eqs. (27) give way to the first three of Eqs. (7) here when all rotors are permitted to be CMGs ($\mathcal{F}=0$, thus $\rho=\mathcal{C}$). After forming the required sum, and replacing their symbols $\underline{\mathrm{L}}$ with $\mathbf{M}$, $\underline{\underline{\mathrm{I}}}$ with $\underline{\underline{\mathbf{I}}}^{S/S^\star}$, $\underline{\underline{\mathrm{I}}}_{\mathrm{p}}$ with $\underline{\underline{\mathbf{I}}}^{R_i/R_i^\star}$, $\underline{\Omega}$ with ${}^N\boldsymbol{\omega}^B$, $\underline{\omega}_{\mathrm{p}}$ with ${}^B\boldsymbol{\omega}^{R_i}$, $(\underline{\dot{\Omega}})_{\mathrm{v}}$ with ${}^N\boldsymbol{\alpha}^B$, and $(\underline{\dot{\omega}}_{\mathrm{p}})_{\mathrm{p}}$ with ${}^B\boldsymbol{\alpha}^{R_i}$, it becomes evident that forming dot products with the resulting expression and three vectors ${}^N\boldsymbol{\omega}_r^B$ produces the first three scalar relationships given by Eqs. (7).

Dynamical Equations for A Complex Gyrostat

A spacecraft known as a simple gyrostat is described in Sec. 3.6 of Ref. [17]; the system S in the preceding discussion becomes a simple gyrostat when the number of flywheels $\mathcal{F}$ is equal to 1, and when no CMGs are present ($\mathcal{C}=0$, $\rho=\mathcal{F}$). A spacecraft with more than one flywheel, such as the one shown in Fig. 2, will be referred to as a complex gyrostat; equations of motion with $\mathcal{F}=6$ are given in the following material.

Without a great loss of generality one can at this point work with six flywheel rotors $R_1,\ldots,R_6$ ($\mathcal{F}=6$) arranged in three counter-rotating pairs as shown in Fig. 2, with the spin axes of R_1 and R_4 parallel to $\hat{\mathbf{b}}_1$, R_2 and R_5 parallel to $\hat{\mathbf{b}}_2$, and R_3 and R_6 parallel to $\hat{\mathbf{b}}_3$. The generalized speeds $u_4,\ldots,u_9$ associated with the flywheels are then used to form the angular velocities ${}^B\boldsymbol{\omega}^{R_i}$ of R_i in B, $(i=1,\ldots,6)$

$$
\begin{aligned}
&{}^B\boldsymbol{\omega}^{R_1}=u_4\hat{\mathbf{b}}_1, \qquad {}^B\boldsymbol{\omega}^{R_2}=u_6\hat{\mathbf{b}}_2, \qquad {}^B\boldsymbol{\omega}^{R_3}=u_8\hat{\mathbf{b}}_3,\\
&{}^B\boldsymbol{\omega}^{R_4}=u_5\hat{\mathbf{b}}_1, \qquad {}^B\boldsymbol{\omega}^{R_5}=u_7\hat{\mathbf{b}}_2, \qquad {}^B\boldsymbol{\omega}^{R_6}=u_9\hat{\mathbf{b}}_3
\end{aligned}
\tag{8}
$$

Up to this point the moment about $R_i^\star$ of forces exerted by B on R_i has been represented by $\mathbf{M}^{B/R_i}$; henceforth we regard the dot product $\mathbf{M}^{B/R_i}\cdot\hat{\boldsymbol{\beta}}_i$ $(i=1,\ldots,\mathcal{F})$ as the sum of two contributions. The first is from a motor-generator, and will be denoted by $\mathbf{M}^{B/R_i}\cdot\hat{\boldsymbol{\beta}}_i$ for convenience. The second is due to damping, related by a constant of proportionality C_d to the angular speed of R_i relative to B. For example, in connection with rotor R_4, $\mathbf{M}^{B/R_4}\cdot\hat{\mathbf{b}}_1$ is replaced by $\mathbf{M}^{B/R_4}\cdot\hat{\mathbf{b}}_1-C_du_5$ in Eqs. (7).

Unit vectors $\hat{\mathbf{b}}_1$, $\hat{\mathbf{b}}_2$, and $\hat{\mathbf{b}}_3$ are taken to be parallel to central principal axes of inertia of S, so that

$$
\underline{\underline{\mathbf{I}}}^{S/S^\star}=I_1\hat{\mathbf{b}}_1\hat{\mathbf{b}}_1+I_2\hat{\mathbf{b}}_2\hat{\mathbf{b}}_2+I_3\hat{\mathbf{b}}_3\hat{\mathbf{b}}_3 \tag{9}
$$

where I_1, I_2, and I_3 are central principal moments of inertia of S. Equations (7) then yield twelve scalar relationships; upon decoupling the first three from the 4th through 9th, they can be written

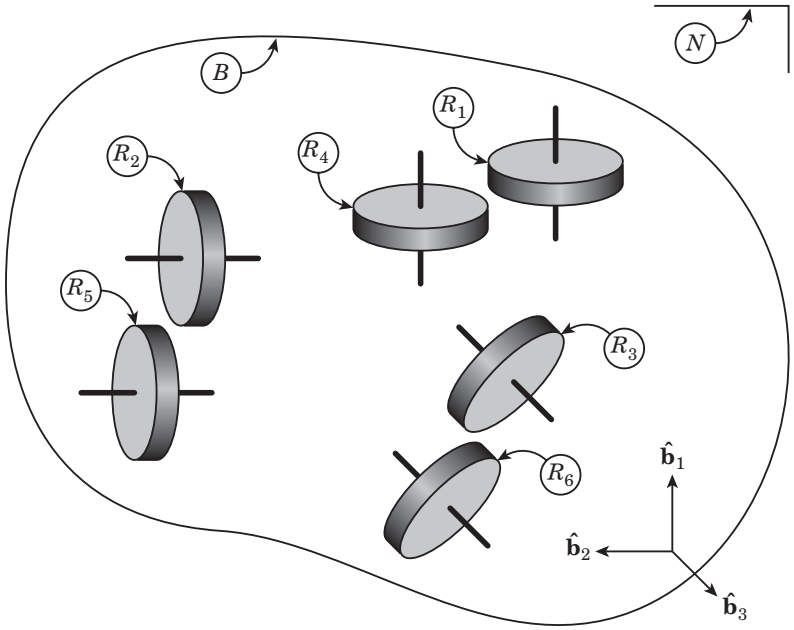

Figure 2: Spacecraft with Flywheels

as

$$(I_1 - 2J)\dot{u}_1 = (I_2 - I_3)u_2u_3 - J[u_2(u_8 + u_9) - u_3(u_6 + u_7)] + M_1 - \left(\mathbf{M}_1 + \mathbf{M}^{B/R_1} + \mathbf{M}_4 + \mathbf{M}^{B/R_4}\right) \cdot \hat{\mathbf{b}}_1 + C_d(u_4 + u_5) \tag{10}$$

$$(I_2 - 2J)\dot{u}_2 = (I_3 - I_1)u_1u_3 - J[u_3(u_4 + u_5) - u_1(u_8 + u_9)] + M_2 - \left(\mathbf{M}_2 + \mathbf{M}^{B/R_2} + \mathbf{M}_5 + \mathbf{M}^{B/R_5}\right) \cdot \hat{\mathbf{b}}_2 + C_d(u_6 + u_7) \tag{11}$$

$$(I_3 - 2J)\dot{u}_3 = (I_1 - I_2)u_1u_2 - J[u_1(u_6 + u_7) - u_2(u_4 + u_5)] + M_3 - \left(\mathbf{M}_3 + \mathbf{M}^{B/R_3} + \mathbf{M}_6 + \mathbf{M}^{B/R_6}\right) \cdot \hat{\mathbf{b}}_3 + C_d(u_8 + u_9) \tag{12}$$

$$J(\dot{u}_1 + \dot{u}_4) = \left(\mathbf{M}_1 + \mathbf{M}^{B/R_1}\right) \cdot \hat{\mathbf{b}}_1 - C_d u_4 \tag{13}$$

$$J(\dot{u}_1 + \dot{u}_5) = \left(\mathbf{M}_4 + \mathbf{M}^{B/R_4}\right) \cdot \hat{\mathbf{b}}_1 - C_d u_5 \tag{14}$$

$$J(\dot{u}_2 + \dot{u}_6) = \left(\mathbf{M}_2 + \mathbf{M}^{B/R_2}\right) \cdot \hat{\mathbf{b}}_2 - C_d u_6 \tag{15}$$

$$J(\dot{u}_2 + \dot{u}_7) = \left(\mathbf{M}_5 + \mathbf{M}^{B/R_5}\right) \cdot \hat{\mathbf{b}}_2 - C_d u_7 \tag{16}$$

$$J(\dot{u}_3 + \dot{u}_8) = \left(\mathbf{M}_3 + \mathbf{M}^{B/R_3}\right) \cdot \hat{\mathbf{b}}_3 - C_d u_8 \tag{17}$$

$$J(\dot{u}_3 + \dot{u}_9) = \left(\mathbf{M}_6 + \mathbf{M}^{B/R_6}\right) \cdot \hat{\mathbf{b}}_3 - C_d u_9 \tag{18}$$

$$m_S \dot{u}_r = F_{r-9} \qquad (r = 10, 11, 12) \tag{19}$$

where J is the central principal moment of inertia of a flywheel rotor for its axis of symmetry, the scalars M_j in Eqs. (10)–(12) are defined by the relationships $M_j \triangleq \mathbf{M} \cdot \hat{\mathbf{b}}_j$, and F_j in Eqs. (19) are defined as $F_j \triangleq \mathbf{F} \cdot \hat{\mathbf{n}}_j$ $(j = 1, 2, 3)$.

Eqs. (10)–(19) are thus a complete set of nonlinear dynamical equations of motion for a complex gyrostat composed of a body B and six axisymmetric rotors $R_1, \ldots, R_6$ whose mass centers and spin axes are fixed in B; the rotors are arranged in pairs, with the spin axes in each pair parallel to each other and to a central principal axis of inertia of the gyrostat.

If a rotor R_i does not possess a magnetic dipole moment, and is housed inside B where it is protected from the action of aerodynamic forces, then the principal contribution to the external torque $\mathbf{M}_i$ is gravitational moment exerted by the celestial body about which the gyrostat orbits. An expression for an often used approximation of gravitational moment is given in Eq. (2.6.8) of Ref. [17], where it becomes clear that the dot products $\mathbf{M}_i \cdot \hat{\mathbf{b}}_i$ and $\mathbf{M}_{i+3} \cdot \hat{\mathbf{b}}_i$ $(i = 1, 2, 3)$ all vanish because in each case the unit vector $\hat{\mathbf{b}}_i$ is parallel to an axis of symmetry of the rotor. After removing rotors R_1, R_2, R_4, R_5, and R_6 from the picture, and setting $C_d = 0$, some manipulation shows that Eqs. (10)–(12) and (17) reduce to Eqs. (3.7.28)–(3.7.31) in Ref. [17] for a simple gyrostat in which the spin axis of the single rotor is parallel to $\hat{\mathbf{b}}_3$.

Approximate, Linear Equations for a Spacecraft with Flywheels and CMGs

In Ref. [3], Wie et al. develop a scheme for controlling a spacecraft's attitude and managing the angular momentum of a collection of CMGs, and the results are applied to a space station. In the case of a spacecraft carrying CMGs and no flywheels ($\mathcal{F} = 0$, $\rho = \mathcal{C}$), the first three of Eqs. (7) can be shown to give rise to the six relationships employed as a basis for control law design in Ref. [3], namely Eqs. (1) and (3) therein. An essential step in the demonstration consists of neglecting the second sum (which receives contributions only from CMGs) in comparison to the first sum appearing in Eqs. (7), based on the assumption that the CMG gimbal speeds are much less than the rotor spin speed. In addition, central moments and products of inertia of S are regarded as constant in Ref. [3], based on the assumption that reorientation of CMG rotors (and gimbals) does not significantly redistribute system mass. Both assumptions are quite reasonable in the case of the International Space Station and its four CMGs with constant rotor speeds of 6,600 rpm.

There are n dynamical equations of motion (7), $n-3$ of which govern rotational motions of B and the CMG rotors. The first three of these are approximated by the three Eqs. (1) of Ref. [3], together with the three additional relationships introduced in Eqs. (3) of Ref. [3] to represent the effects of CMGs. This approach does not account entirely for all $n - 6$ of Eqs. (7) that must follow from the third sum therein, where $n - 6$ is equal to the number of gimbals (revolute joints) supporting the CMG rotors in B; however, for the purpose of designing a control law the approach can be extended to represent the effects of flywheels in a similar manner. There results nine approximate dynamical equations for a spacecraft with flywheels and CMGs. To describe the orientation of B in a local vertical, local horizontal reference frame L, one may choose a body-three, 2-3-1 rotation sequence as set forth on p. 423 of Ref. [17]. The sequence is also known as pitch-yaw-roll, with the angles denoted by θ_1, θ_2, and θ_3 respectively, and there are three associated kinematical equations of motion. The set of twelve equations can be linearized about an Earth-pointing motion associated with a circular orbit of rate n, and written as

$$I_1 \dot{\tilde{u}}_1 = (I_3 - I_2)(3n^2 \tilde{\theta}_3 + n\tilde{u}_3) - \tau_1 - \bar{\tau}_1 + w_1 \tag{20}$$

$$I_2 \dot{\tilde{u}}_2 = (I_3 - I_1)(3n^2 \tilde{\theta}_1) - \tau_2 - \bar{\tau}_2 + w_2 \tag{21}$$

$$I_3 \dot{\tilde{u}}_3 = (I_2 - I_1) n\tilde{u}_1 - \tau_3 - \bar{\tau}_3 + w_3 \tag{22}$$

$$\dot{\tilde{h}}_1 = n\tilde{h}_3 + \tau_1, \qquad \dot{\tilde{h}}_2 = \tau_2, \qquad \dot{\tilde{h}}_3 = -n\tilde{h}_1 + \tau_3 \tag{23}$$

$$\dot{\tilde{H}}_1 = n\tilde{H}_3 + \bar{\tau}_1, \qquad \dot{\tilde{H}}_2 = \bar{\tau}_2, \qquad \dot{\tilde{H}}_3 = -n\tilde{H}_1 + \bar{\tau}_3 \tag{24}$$

$$\dot{\tilde{\theta}}_1 = \tilde{u}_2, \qquad \dot{\tilde{\theta}}_2 = \tilde{u}_3 - n\tilde{\theta}_3, \qquad \dot{\tilde{\theta}}_3 = \tilde{u}_1 + n\tilde{\theta}_2 \tag{25}$$

where all quantities with a tilde over them are referred to as perturbations, and considered "small." The moment $\mathbf{M}$ is regarded as the sum of two terms, the gravitational moment exerted on S and reflected in the terms with a coefficient of $3n^2$, as well as all other contributions $\mathbf{w}$, with $w_r \triangleq \mathbf{w} \cdot \hat{\mathbf{b}}_r$ $(r = 1, 2, 3)$. The scalars τ_r are defined in terms of the contributions from CMGs to the first sum in Eqs. (7),

$$\begin{aligned} \tau_r &\triangleq \boldsymbol{\tau} \cdot \hat{\mathbf{b}}_r \triangleq \sum_{i=\mathcal{F}+1}^{\rho} \left(\frac{{}^B d}{dt} {}^B\mathbf{H}^{R_i/R_i^\star} + {}^N\boldsymbol{\omega}^B \times {}^B\mathbf{H}^{R_i/R_i^\star} \right) \cdot \hat{\mathbf{b}}_r \\ &= \left[\frac{{}^B d}{dt} \left(\sum_{i=\mathcal{F}+1}^{\rho} {}^B\mathbf{H}^{R_i/R_i^\star} \right) + {}^N\boldsymbol{\omega}^B \times \left(\sum_{i=\mathcal{F}+1}^{\rho} {}^B\mathbf{H}^{R_i/R_i^\star} \right) \right] \cdot \hat{\mathbf{b}}_r \qquad (r = 1, 2, 3) \end{aligned} \tag{26}$$

The scalars $\tilde{h}_r$ and $\dot{\tilde{h}}_r$ denote the perturbations of the quantities

$$h_r \triangleq \mathbf{h} \cdot \hat{\mathbf{b}}_r \triangleq \left(\sum_{i=\mathcal{F}+1}^{\rho} {}^B\mathbf{H}^{R_i/R_i^\star} \right) \cdot \hat{\mathbf{b}}_r, \qquad \dot{h}_r \triangleq \frac{d}{dt} h_r \qquad (r = 1, 2, 3) \tag{27}$$

The scalars $\bar{\tau}_r$, $\tilde{H}_r$, and $\dot{\tilde{H}}_r$, and the vectors $\bar{\boldsymbol{\tau}}$ and $\mathbf{H}$, associated with flywheels, are involved in similar relationships with the limits of the sums going from 1 to $\mathcal{F}$, rather than from $\mathcal{F}+1$ to ρ.

Equations (20)–(25) are supplemented with differential equations governing $\int \tilde{h}_r \, dt$ and $\int \tilde{H}_r \, dt$, $(r = 1, 2, 3)$ such as those introduced in Ref. [3] to eliminate biases in the time histories of the integrands. These relationships become better suited for control law design after they have been made nondimensional by use of the following definitions,

$$\theta_i^* \triangleq \tilde{\theta}_i, \qquad u_i^* \triangleq \frac{\tilde{u}_i}{n}, \qquad h_i^* \triangleq \frac{\tilde{h}_i}{I_i \, n}, \qquad H_i^* \triangleq \frac{\tilde{H}_i}{I_i \, n} \qquad (i = 1, 2, 3) \tag{28}$$

$$\tau_i^* \triangleq \frac{\tau_i}{I_i \, n^2}, \qquad \bar{\tau}_i^* \triangleq \frac{\bar{\tau}_i}{I_i \, n^2}, \qquad w_i^* \triangleq \frac{w_i}{I_i \, n^2} \qquad (i = 1, 2, 3) \tag{29}$$

$$t^* \triangleq nt \tag{30}$$

The 18 nondimensional, linear differential equations can be written in the form required for application of the Linear Quadratic Regulator technique,

$$\{\dot{x}\} = [A] \{x\} + [B] \{\tau\} + \{W\} \tag{31}$$

to obtain a linear controller design with the goal of determining the values of $\boldsymbol{\tau}$ and $\bar{\boldsymbol{\tau}}$ that best control the orientation of B in L, and minimize the magnitudes of $\mathbf{h}$ and $\mathbf{H}$. The column matrix $\{\tau\}$ is dimensioned 6×1 with the elements

$$\{\tau\} \triangleq [\ \tau_1^* \quad \tau_2^* \quad \tau_3^* \quad \bar{\tau}_1^* \quad \bar{\tau}_2^* \quad \bar{\tau}_3^*\ ]^{\mathrm{T}} \tag{32}$$

where the superscript T indicates the transpose of a matrix.

FLYWHEEL STEERING LAWS

The great benefit of utilizing flywheels is that they can serve simultaneously as attitude control actuators and as energy storage devices; this dual role requires that $\bar{\boldsymbol{\tau}}$, obtained on the basis of

attitude control considerations, be applied in a way that allows energy to be stored or discharged as needed. A flywheel rotor R_i is suspended in a vacuum housing in B with magnetic bearings, and relative motion between R_i and B is brought about by a motor-generator that enables B to exert on R_i a torque with magnitude $\mathbf{M}^{B/R_i} \cdot \hat{\boldsymbol{\beta}}_i$, the purpose of which is to produce and change rotor momentum in order to furnish attitude control, and to alter the rotor's rotational kinetic energy. An important measure of energy storage is power, or the rate at which rotational kinetic energy is changed. In this section relationships for $\mathbf{M}^{B/R_i} \cdot \hat{\boldsymbol{\beta}}_i$ as functions of power, $\overline{\boldsymbol{\tau}}$, and rotor speeds are developed; they are referred to collectively as a *flywheel steering law* because they are similar in nature to a CMG steering law that determines gimbal speeds (and thus, indirectly, gimbal motor torques) needed to produce $\boldsymbol{\tau}$ as requested by a control law. Two such steering laws are presented; the first is the result of simply prescribing the total power of the flywheel system, whereas specification of the power required for each of three flywheel pairs gives rise to the second law. Bearing friction and damping are neglected in the design of the steering laws.

The flywheel rotors are arranged in counter-rotating pairs; each pair, denoted by F_i, consists of rotors R_i and R_{i+3} $(i = 1, 2, 3)$. Referring to Eq. (5) of Ref. [18], the power ${}^B P^{F_i}$ of F_i in B can be expressed as

$$ {}^B P^{F_i} = \left(\underline{\mathbf{I}}^{R_i/R_i^\star} \cdot {}^B\boldsymbol{\alpha}^{R_i} \right) \cdot {}^B\boldsymbol{\omega}^{R_i} + \left(\underline{\mathbf{I}}^{R_{i+3}/R_{i+3}^\star} \cdot {}^B\boldsymbol{\alpha}^{R_{i+3}} \right) \cdot {}^B\boldsymbol{\omega}^{R_{i+3}} \qquad (i = 1, 2, 3) \tag{33} $$

or, in view of Eqs. (8),

$$ {}^B P^{F_i} = J \left(\dot{u}_{2i+2} u_{2i+2} + \dot{u}_{2i+3} u_{2i+3} \right) \qquad (i = 1, 2, 3) \tag{34} $$

and therefore the total power may be expressed as

$$ {}^B P^F \triangleq \sum_{i=1}^{3} {}^B P^{F_i} = J \sum_{i=1}^{3} \left(\dot{u}_{2i+2} u_{2i+2} + \dot{u}_{2i+3} u_{2i+3} \right) \tag{35} $$

Now, if $\dot{u}_1$, $\dot{u}_2$, and $\dot{u}_3$ are assumed to be small in comparison to $\dot{u}_4, \ldots, \dot{u}_9$, C_d is neglected, and $\mathbf{M}_i \cdot \hat{\mathbf{b}}_i$ and $\mathbf{M}_{i+3} \cdot \hat{\mathbf{b}}_i$ $(i = 1, 2, 3)$ vanish for the reasons put forth earlier, then Eqs. (13)–(18) may be approximated as

$$ J\dot{u}_{2i+2} \approx \mathbf{M}^{B/R_i} \cdot \hat{\mathbf{b}}_i, \qquad J\dot{u}_{2i+3} \approx \mathbf{M}^{B/R_{i+3}} \cdot \hat{\mathbf{b}}_i \qquad (i = 1, 2, 3) \tag{36} $$

which, together with the counterparts to Eqs. (26) and (27), lead to

$$ \begin{aligned} (\overline{\boldsymbol{\tau}} - {}^N\boldsymbol{\omega}^B \times \mathbf{H}) \cdot \hat{\mathbf{b}}_i = \dot{H}_i &= J(\dot{u}_{2i+2} + \dot{u}_{2i+3}) \\ &\approx \left(\mathbf{M}^{B/R_i} + \mathbf{M}^{B/R_{i+3}} \right) \cdot \hat{\mathbf{b}}_i \qquad (i = 1, 2, 3) \end{aligned} \tag{37} $$

or

$$ \mathbf{M}^{B/R_{i+3}} \cdot \hat{\mathbf{b}}_i \approx \left(\overline{\boldsymbol{\tau}} - {}^N\boldsymbol{\omega}^B \times \mathbf{H} - \mathbf{M}^{B/R_i} \right) \cdot \hat{\mathbf{b}}_i \qquad (i = 1, 2, 3) \tag{38} $$

Substitution from Eqs. (36) into Eq. (35) produces

$$ {}^B P^F \approx \sum_{i=1}^{3} \left(u_{2i+2} \mathbf{M}^{B/R_i} + u_{2i+3} \mathbf{M}^{B/R_{i+3}} \right) \cdot \hat{\mathbf{b}}_i \tag{39} $$

Eqs. (38) and (39) constitute a system of four equations, linear in the six unknowns $\mathbf{M}^{B/R_i} \cdot \hat{\mathbf{b}}_i$ and $\mathbf{M}^{B/R_{i+3}} \cdot \hat{\mathbf{b}}_i$, $(i = 1, 2, 3)$. This underdetermined system can be written in matrix form as

$$ [A_s] \{y\} = \{z\} \tag{40} $$

where

$$[A_s] \triangleq \begin{bmatrix} 1 & 1 & 0 & 0 & 0 & 0 \\ 0 & 0 & 1 & 1 & 0 & 0 \\ 0 & 0 & 0 & 0 & 1 & 1 \\ u_4 & u_5 & u_6 & u_7 & u_8 & u_9 \end{bmatrix} \tag{41}$$

$$\{y\} \triangleq \begin{bmatrix} \mathbf{M}^{B/R_1} \cdot \hat{\mathbf{b}}_1 & \mathbf{M}^{B/R_4} \cdot \hat{\mathbf{b}}_1 & \mathbf{M}^{B/R_2} \cdot \hat{\mathbf{b}}_2 & \mathbf{M}^{B/R_5} \cdot \hat{\mathbf{b}}_2 & \mathbf{M}^{B/R_3} \cdot \hat{\mathbf{b}}_3 & \mathbf{M}^{B/R_6} \cdot \hat{\mathbf{b}}_3 \end{bmatrix}^{\mathrm{T}} \tag{42}$$

$$\{z\} \triangleq \begin{bmatrix} (\overline{\boldsymbol{\tau}} - {}^{N}\boldsymbol{\omega}^{B} \times \mathbf{H}) \cdot \hat{\mathbf{b}}_1 & (\overline{\boldsymbol{\tau}} - {}^{N}\boldsymbol{\omega}^{B} \times \mathbf{H}) \cdot \hat{\mathbf{b}}_2 & (\overline{\boldsymbol{\tau}} - {}^{N}\boldsymbol{\omega}^{B} \times \mathbf{H}) \cdot \hat{\mathbf{b}}_3 & {}^{B}P^{F} \end{bmatrix}^{\mathrm{T}} \tag{43}$$

One may solve Eqs. (40) by forming a matrix pseudo-inverse such as the one presented in Ref. [19] and developed by Moore and Penrose for underdetermined systems,

$$[A_s]^{+} \triangleq [A_s]^{\mathrm{T}} \left([A_s] [A_s]^{\mathrm{T}} \right)^{-1} \tag{44}$$

which yields the solution

$$\{y\} = [A_s]^{+} \{z\} \tag{45}$$

that minimizes the sum of the squares of the unknowns, $\{y\}^{\mathrm{T}} \{y\}$. (There exist several other performance measures that could be considered in solving an underdetermined system of equations.) Use of a pseudo-inverse is in essence the suggestion made by Hall in Sec. 4 of Ref. [7], yielding a steering law wherein the power and attitude control requirements are met simultaneously, and a function of the instantaneous motor torques, the sum $\sum_{i=1}^{3} [(\mathbf{M}^{B/R_i} \cdot \hat{\mathbf{b}}_i)^2 + (\mathbf{M}^{B/R_{i+3}} \cdot \hat{\mathbf{b}}_i)^2]$, is minimized.

Upon making the definitions

$$d_1 \triangleq u_5 - u_4, \qquad d_2 \triangleq u_7 - u_6, \qquad d_3 \triangleq u_9 - u_8 \tag{46}$$

$$s_1 \triangleq u_5 + u_4, \qquad s_2 \triangleq u_7 + u_6, \qquad s_3 \triangleq u_9 + u_8 \tag{47}$$

the pseudo-inverse can be written explicitly as

$$[A_s]^{+} = \tag{48}$$

$$\frac{1}{2\left(d_1{}^2 + d_2{}^2 + d_3{}^2\right)} \begin{bmatrix} 2u_5 d_1 + d_2{}^2 + d_3{}^2 & s_2 d_1 & s_3 d_1 & -2d_1 \\ -2u_4 d_1 + d_2{}^2 + d_3{}^2 & -s_2 d_1 & -s_3 d_1 & 2d_1 \\ s_1 d_2 & 2u_7 d_2 + d_1{}^2 + d_3{}^2 & s_3 d_2 & -2d_2 \\ -s_1 d_2 & -2u_6 d_2 + d_1{}^2 + d_3{}^2 & -s_3 d_2 & 2d_2 \\ s_1 d_3 & s_2 d_3 & 2u_9 d_3 + d_1{}^2 + d_2{}^2 & -2d_3 \\ -s_1 d_3 & -s_2 d_3 & -2u_8 d_3 + d_1{}^2 + d_2{}^2 & 2d_3 \end{bmatrix}$$

It is worth noting that if the rotor speed differences d_1, d_2, and d_3 vanish for all three flywheel pairs, the pseudo-inverse becomes infinite and the steering law does not furnish a result. Since the rotor speeds of the flywheels in each pair will normally have opposite signs, this condition should be unlikely. In addition, examination of Eqs. (42), (43), (45), and (48) reveals that when the flywheels are not required to provide attitude control ($\overline{\boldsymbol{\tau}} = \mathbf{0}$), and the condition of counter-rotation is present ($u_{2i+3} = -u_{2i+2}$, thus $\mathbf{H} = \mathbf{0}$), this steering law dictates that $\mathbf{M}^{B/R_{i+3}} \cdot \hat{\mathbf{b}}_i = -\mathbf{M}^{B/R_i} \cdot \hat{\mathbf{b}}_i$, and counter-rotation is preserved.

As an alternative to dealing with the four Eqs. (38) and (39), one could replace the single Eq. (39) with three others by choosing to divide the power requirement evenly among the three flywheel pairs, ${}^{B}P^{F_1} = {}^{B}P^{F_2} = {}^{B}P^{F_3} = \frac{1}{3}\,{}^{B}P^{F}$, yielding six equations in six unknowns. Substitution from Eqs. (36) into Eqs. (34) gives the three new equations

$$ {}^{B}P^{F_i} \approx \left(u_{2i+2}\mathbf{M}^{B/R_i} + u_{2i+3}\mathbf{M}^{B/R_{i+3}} \right) \cdot \hat{\mathbf{b}}_i \qquad (i = 1, 2, 3) \tag{49} $$

Now, substitution from Eqs. (38) gives

$$ \begin{aligned} {}^{B}P^{F_i} &\approx u_{2i+2}\left(\mathbf{M}^{B/R_i} \cdot \hat{\mathbf{b}}_i \right) + u_{2i+3}\left(\overline{\boldsymbol{\tau}} - {}^{N}\boldsymbol{\omega}^{B} \times \mathbf{H} - \mathbf{M}^{B/R_i} \right) \cdot \hat{\mathbf{b}}_i \\ &= (u_{2i+2} - u_{2i+3})\left(\mathbf{M}^{B/R_i} \cdot \hat{\mathbf{b}}_i \right) + u_{2i+3}\left(\overline{\boldsymbol{\tau}} - {}^{N}\boldsymbol{\omega}^{B} \times \mathbf{H} \right) \cdot \hat{\mathbf{b}}_i \quad (i = 1, 2, 3) \end{aligned} \tag{50} $$

which can be rearranged to yield

$$ \mathbf{M}^{B/R_i} \cdot \hat{\mathbf{b}}_i = \frac{ {}^{B}P^{F_i} - u_{2i+3}\left(\overline{\boldsymbol{\tau}} - {}^{N}\boldsymbol{\omega}^{B} \times \mathbf{H} \right) \cdot \hat{\mathbf{b}}_i}{u_{2i+2} - u_{2i+3}} \qquad (i = 1, 2, 3) \tag{51} $$

and, when one substitutes from this expression into Eq. (38), the result is

$$ \mathbf{M}^{B/R_{i+3}} \cdot \hat{\mathbf{b}}_i = \frac{u_{2i+2}\left(\overline{\boldsymbol{\tau}} - {}^{N}\boldsymbol{\omega}^{B} \times \mathbf{H} \right) \cdot \hat{\mathbf{b}}_i - {}^{B}P^{F_i}}{u_{2i+2} - u_{2i+3}} \qquad (i = 1, 2, 3) \tag{52} $$

Eqs. (51) and (52) constitute another flywheel steering law, indicating the moment that must be applied by a motor-generator to each of two rotors belonging to a counter-rotating pair in order to apply $\overline{\boldsymbol{\tau}}$ as called for by an attitude control law, and at the same time satisfy power requirements specified by ${}^{B}P^{F_i}$. Each flywheel pair is expected to operate with the sign of the rotor speed u_{2i+3} opposite the sign of u_{2i+2}; hence, the denominators $u_{2i+2} - u_{2i+3}$ should remain well away from zero. In the event that the flywheels are not required to participate in attitude control, and the condition of counter-rotation is present, the steering law yields $\mathbf{M}^{B/R_{i+3}} \cdot \hat{\mathbf{b}}_i = -\mathbf{M}^{B/R_i} \cdot \hat{\mathbf{b}}_i$ and thus maintains the condition of counter-rotation.

LINEAR CONTROLLER

A law for controlling the orientation of B in L, and the momentum of flywheels and CMGs, has been designed using the infinite-horizon Linear Quadratic Regulator technique, in which a scalar quadratic performance index given by

$$ \mathcal{P} = \int_0^\infty \left(\{x\}^{\mathrm{T}} [Q] \{x\} + \{\tau\}^{\mathrm{T}} [R] \{\tau\} \right) dt \tag{53} $$

is minimized subject to the linear Eqs. (31) with $\{W\} = \{0\}$. The technique yields a state feedback gain matrix $[K]$ which in turn is used to obtain $\{\tau\}$,

$$ \{\tau\} = -[K]\{x\} \tag{54} $$

As suggested by Bryson and Ho in Ref. [20], the weighting matrix $[Q]$ can be chosen as diagonal, and unity should be approximately equal to the product of Q_{jj} and the square of the maximum acceptable value of the associated element x_j of $\{x\}$. Maximum acceptable values of several parameters used in constructing $[Q]$ are listed in Table 1. Before constructing $[Q]$, the values in Table 1 must be made nondimensional to be in correspondence with the elements of $\{x\}$. Likewise, a diagonal form of $[R]$ is convenient, with unity approximately equal to the product of R_{kk} and the square of the maximum acceptable value of the associated element of $\{\tau\}$ ($k = 1, \ldots, 6$). The maximum expected value of each element of $\{\tau\}$ is taken to be 2.7 N-m, which must be nondimensionalized before constructing $[R]$.

Table 1: Maximum Acceptable Values

Parameter ($i = 1, 2, 3$)	Max Value
$\tilde{\theta}_i$	1 deg
$\tilde{u}_i$	0.2 deg/s
$\tilde{h}_i$	6,779 N-m-s
$\tilde{H}_i$	6,779 N-m-s
$\int \tilde{h}_i dt$	2.7×10^6 N-m-s^2
$\int \tilde{H}_i dt$	2.7×10^6 N-m-s^2

Simulation Parameters

Other values required for a numerical simulation are as follows.

Moments and products of inertia of S with respect to $S^\star$ are taken to be

$$\left[I^{S/S^\star}\right] = 1.36 \times \begin{bmatrix} 50.28 & -0.39 & -0.24 \\ -0.39 & 10.80 & 0.16 \\ -0.24 & 0.16 & 58.57 \end{bmatrix} \times 10^6 \text{ kg-m}^2 \tag{55}$$

which are the same values (in metric units) as those associated with Phase 1 in Table 1 of Ref. [3], with the exception of I_{13} which is suspected to be a typographical error, the correct value being -0.24×10^6 slug-ft^2.

The value of $\mathbf{w}$ used in Ref. [3] represents the moment about $S^\star$ of aerodynamic forces exerted on the Phase 1 configuration of S when the attitude is near TEA; it is given by

$$\mathbf{w} = 1.36[(1 + \sin nt + \frac{1}{2}\sin 2nt)\hat{\mathbf{b}}_1 + (4 + 2\sin nt + \frac{1}{2}\sin 2nt)\hat{\mathbf{b}}_2 + (1 + \sin nt + \frac{1}{2}\sin 2nt)\hat{\mathbf{b}}_3] \text{ N-m} \tag{56}$$

where n, the magnitude of ${}^N\boldsymbol{\omega}^L$, is taken to be 0.001131 rad/s.

Each flywheel pair in the FESS is required to discharge 4,400 W of power during the portion of the orbit that lies within the Earth's shadow, known as the period of eclipse. The remaining portion of the orbit, during which sunlight reaches the spacecraft, is taken to be twice as long as the eclipse. Therefore, for each orbit, the total power that must be supplied by the 48 pairs of flywheels in the physical system is given by

$${}^B\bar{P}^F = \begin{cases} 48 \times \quad 2,200 \text{ W} = \quad 105.6 \text{ kW} & 0 \le t \le \frac{2}{3}\frac{2\pi}{n} \quad \text{(charge)} \\ 48 \times -4,400 \text{ W} = -211.2 \text{ kW} & \frac{2}{3}\frac{2\pi}{n} \le t \le \frac{2\pi}{n} \quad \text{(discharge)} \end{cases} \tag{57}$$

where the bar over P indicates a known function of t to be used in connection with the pseudo-inverse steering law developed previously. The alternative steering law is referred to as a divided power law because the power requirement is divided into three equal parts, therefore ${}^B\bar{P}^{F_1} = {}^B\bar{P}^{F_2} = {}^B\bar{P}^{F_3} = \frac{1}{3}{}^B\bar{P}^F$, or

$${}^B\bar{P}^{F_i} = \begin{cases} 35.2 \text{ kW} & 0 \le t \le \frac{2}{3}\frac{2\pi}{n} \quad \text{(charge)} \\ -70.4 \text{ kW} & \frac{2}{3}\frac{2\pi}{n} \le t \le \frac{2\pi}{n} \quad \text{(discharge)} \end{cases} \qquad (i = 1, 2, 3) \tag{58}$$

The FESS would have been made up of 96 flywheels; since the present model involves only 6 rotors, a scaling factor of $96/6 = 16$ is used; thus $J = 16 \times 0.3010$ kg-m^2 $= 4.82$ kg-m^2.

Energy Feedback

The power possessed by the flywheels, given in Eq. (35), can differ from the value required by Eq. (57) when $C_d \neq 0$. If left unchecked, such unwanted resistance or damping will lead to a difference between ${}^B P^F$ and ${}^B \bar{P}^F$ that increases with time, to rotor speeds that exceed their maximum and minimum limits, and to singularities in the steering laws. These deleterious effects of damping can be eliminated by the control system through feedback of rotational kinetic energy error.

The total rotational kinetic energy ${}^B K^F$ of the flywheel rotors relative to B can be expressed as

$$ {}^B K^F = \frac{J}{2} \sum_{i=4}^{9} {u_i}^2 \tag{59} $$

and the power of F in B is given by the derivative of ${}^B K^F$ with respect to t,

$$ {}^B P^F = \frac{d}{dt} {}^B K^F \tag{60} $$

One can regard the required power ${}^B \bar{P}^F$ as the time derivative of a required kinetic energy of F in B

$$ {}^B \bar{P}^F = \frac{d}{dt} {}^B \bar{K}^F \tag{61} $$

and define a kinetic energy error e_k as the quantity

$$ e_k \triangleq {}^B K^F - {}^B \bar{K}^F \tag{62} $$

that is governed by the differential equation

$$ \dot{e}_k = \frac{d}{dt} \left({}^B K^F - {}^B \bar{K}^F \right) = {}^B P^F - {}^B \bar{P}^F \triangleq e_p \tag{63} $$

where e_p is defined to be the error in power, or the difference between the actual and required values. The LQR technique can be used to control the kinetic energy error by minimizing the cost function

$$ \mathcal{P}_E = \int_0^\infty \left(\lambda \, {e_k}^2 + {e_p}^2 \right) dt \tag{64} $$

where λ is a weighting parameter on the kinetic energy error of the flywheel system. This leads to a feedback controller in which the required power is adjusted by the amount $-\sqrt{\lambda}\, e_k$. Thus, the *commanded* power is defined to be

$$ {}^B P_c^F \triangleq {}^B \bar{P}^F - \sqrt{\lambda}\, e_k \tag{65} $$

and is used in place of ${}^B P^F$ in Eq. (43) for the pseudo-inverse steering law. Similarly, a commanded power ${}^B P_c^{F_i}$ $(i = 1, 2, 3)$ is obtained for each of the three flywheel pairs and used together with Eqs. (51) and (52) for the divided power steering law. The merits of this kinetic energy error feedback are illustrated presently.

Control System Block Diagram

The block diagram in Fig. 3 shows the LQR (controller), flywheel steering law, and kinetic energy error feedback arranged to form a complete control system in `MATLAB/Simulink`®. The differential

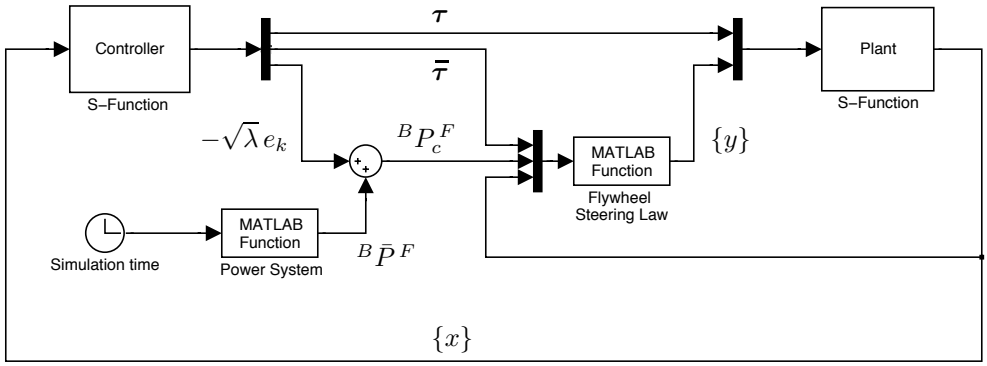

Figure 3: Control System Block Diagram

equations governing the behavior of the plant model are placed in a `Simulink`® S-Function to be numerically integrated and provide the value of the state $\{x\}$ at the current simulation time. The current value of the state is fed to the controller S-Function, where it is made nondimensional and then multiplied by the LQR-derived state feedback gain matrix to generate the control torques $\boldsymbol{\tau}$ and $\overline{\boldsymbol{\tau}}$. The controller also determines the kinetic energy error of the flywheel system, e_k, needed to calculate the commanded power, ${}^B P_c^{\,F}$, that is used together with the flywheel control torque $\overline{\boldsymbol{\tau}}$ in the flywheel steering law to obtain the flywheel motor torque measure numbers in $\{y\}$ [see Eq. (42)]. These are supplied to the plant model, and the control loop cycle is repeated. (The subject of CMG steering is well understood; therefore, our simulations do not include a model of individual CMG gimbal motions.)

TEA Seeking

The Torque Equilibrium Attitude (TEA) of a spacecraft is defined as the orientation for which the angular acceleration of B in N vanishes. The present ISS attitude and CMG momentum control algorithm can keep the orientation in the neighborhood of a time-varying TEA almost indefinitely, without requiring any expenditure of propellant from the Reaction Control System. In what follows, the design of a control law that seeks TEA with CMGs and flywheels is described briefly, and then simulation results are presented that illustrate the performance and features of our control and steering laws. We first illustrate the consequences of failing to counteract damping, and then demonstrate the advantages of kinetic energy error feedback.

Seeking a TEA requires regulating the states contained in the 18×1 column matrix

$$\{x\} = [\ \theta_1^*,\quad \theta_2^*,\quad \theta_3^*,\quad u_1^*, \ldots,\quad h_1^*, \ldots,\quad H_1^*, \ldots,\quad \int h_1^* dt^*, \ldots,\quad \int H_1^* dt^*, \ldots\ ]^{\mathrm{T}} \tag{66}$$

Weighting matrices $[Q]$ and $[R]$ are constructed with the associated values presented previously. The matrices $[A]$, $[Q]$, and $[B]$ are dimensioned 18×18, 18×18, and 18×6, respectively, in accordance with the number of regulated state variables for this control scheme.

Simulation results for this control law, discussed in the remainder of this section, are obtained with the following initial values of the state variables. Angles describing the orientation of B in L at $t = t_0$ are $\theta_1(t_0) = 5^\circ$ (pitch), $\theta_2(t_0) = 5^\circ$ (yaw), and $\theta_3(t_0) = 5^\circ$ (roll). Angular speeds associated with ${}^N\boldsymbol{\omega}^{\,B}$ (with ${}^L\boldsymbol{\omega}^{\,B} = \mathbf{0}$) are $u_1(t_0) = -9.86 \times 10^{-5}$ rad/s, $u_2(t_0) = -1.12 \times 10^{-3}$ rad/s, and $u_3(t_0) = 9.82 \times 10^{-5}$ rad/s. Rotor spin speeds are $u_4(t_0) = u_6(t_0) = u_8(t_0) = -20,000$ rpm, and $u_5(t_0) = u_7(t_0) = u_9(t_0) = 20,000$ rpm. Initial values of CMG momentum measure numbers are $h_1(t_0) = h_2(t_0) = h_3(t_0) = 0$.

Damped Flywheel Rotors

The detrimental effects of damping are brought to light by performing a simulation with an illustrative value of $C_d = 10^{-5}$ N-m-s. One might be tempted to neglect such a seemingly small effect, especially over the short term, but it is shown here to be troublesome if not dealt with over long periods. The performance of the TEA-seeking control law without feedback of kinetic energy error is recorded in Figs. 4–7.

Figure 4 shows the time history of the attitude angles and the inertial angular velocity. The solid curve is used for θ_1 (pitch), the dashed curve for θ_2 (yaw), and the dash-dot curve is used for θ_3 (roll). The average values of these orientation angles in the steady state are referred to as average torque equilibrium attitude angles, and are approximately the same as those shown in Ref. [3], -7.5° in pitch, -1.2° in yaw, and -0.2° in roll. The amplitudes of the steady state oscillations can be reduced significantly with cyclic disturbance rejection filters, as shown in Ref. [3]. The lower plot of Fig. 4 shows the inertial angular velocity response, with u_1, u_2, and u_3, shown with solid, dashed, and dash-dot curves respectively. Although they are not shown, plots of the magnitudes of $\mathbf{h}$ and $\mathbf{H}$ are virtually identical, remain below 14,000 N-m-s over the first orbit, and in the steady state remain well below 4,745 N-m-s, the capacity of a single ISS CMG.

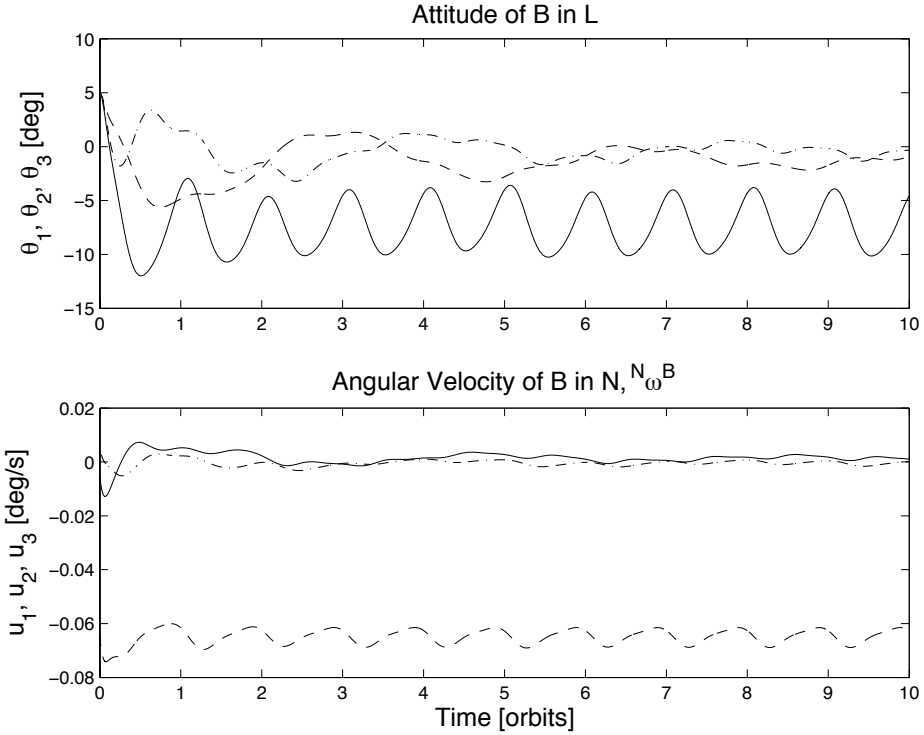

Figure 4: Attitude, Angular Velocity with Damped Flywheel Rotors

The upper plot of Fig. 5 contains the actual power delivered to the spacecraft by the flywheel system as a function of time. The middle plot displays the error between the actual power and the required power due to the damping in the flywheel system, which leads to the large secular kinetic energy loss of more than 50,000 kJ after 10 orbits, shown in the lower plot.

The kinetic energy error of the flywheel system is reflected in the angular speeds of the flywheels relative to B shown in Fig. 6. Speeds of the flywheel pair whose spin axes are parallel to $\hat{\mathbf{b}}_1$ are contained in the upper plots, with u_4 represented by the solid curve, and u_5 indicated by the dashed;

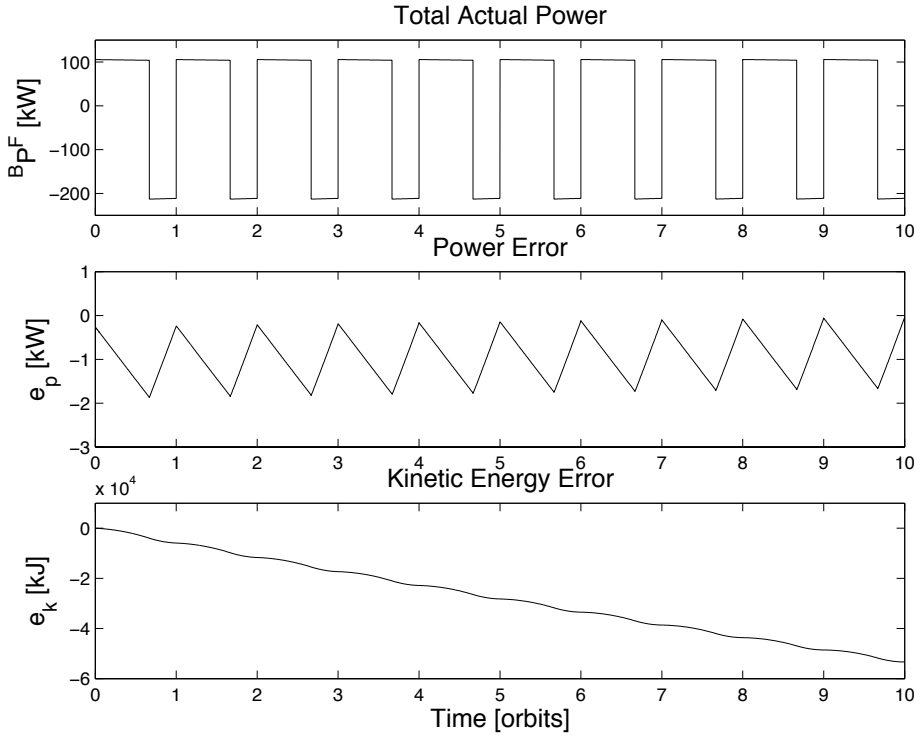

Figure 5: Power, Power Error, Kinetic Energy Error with Damped Flywheel Rotors

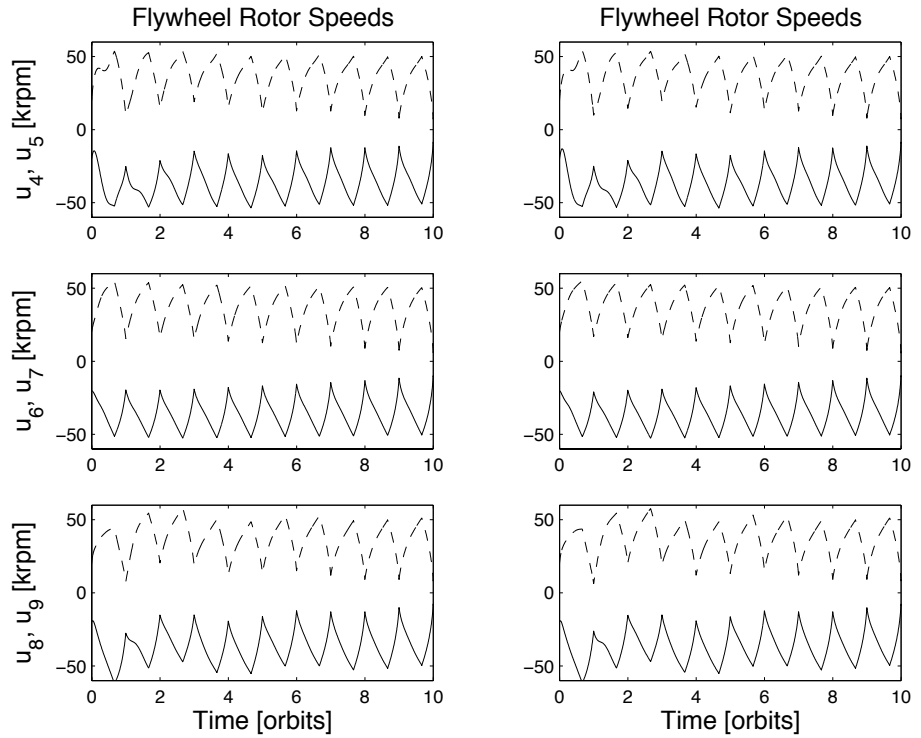

Figure 6: Flywheel Angular Speeds with Damped Flywheel Rotors (Pseudo-Inverse left, Divided Power right)

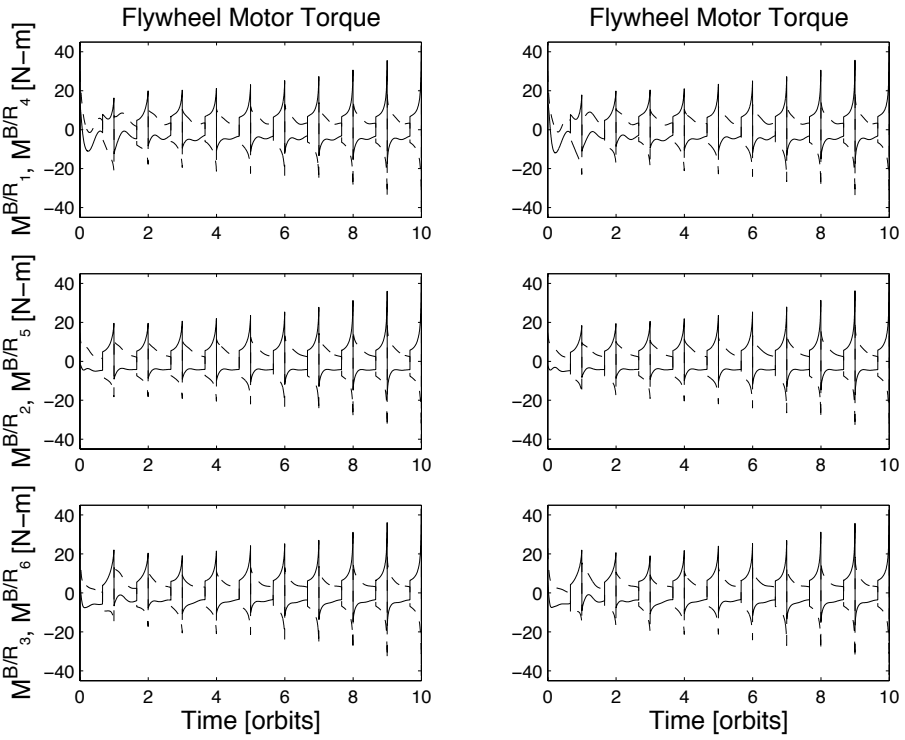

Figure 7: Flywheel Motor Torque with Damped Flywheel Rotors

speeds of the pairs whose spin axes are parallel to $\hat{\mathbf{b}}_2$ and $\hat{\mathbf{b}}_3$ are depicted in the middle and lower plots, respectively. The flywheel rotor speeds exhibit a secular decay. No significant difference appears between the behavior resulting from the pseudo-inverse and divided power steering laws, presented in the left and right columns, respectively.

Time histories of flywheel motor torques, in the presence of damping, are displayed in Fig. 7 where the results in the left and right columns are associated with the pseudo-inverse and divided power steering laws, respectively. A solid curve is used for $\mathbf{M}^{B/R_i} \cdot \hat{\mathbf{b}}_i$ $(i = 1, 2, 3)$, and a dashed curve for $\mathbf{M}^{B/R_i} \cdot \hat{\mathbf{b}}_{i-3}$ $(i = 4, 5, 6)$. The effects of damping appear to be negligible at first; however, after some time it is apparent that damping causes the motor torque magnitudes to increase, with either steering law. Inspection of Eq. (39) indicates that the secular decay in rotor speeds requires an increase in motor torques in order to produce the required power. The increase in motor torque magnitudes implies further power losses as more electrical power must be diverted to the motor-generators in order to meet the attitude control and power management requirements simultaneously.

Counteracting Damping with Kinetic Energy Error Feedback

To compensate for damping, the kinetic energy error feedback design is employed with a weighting parameter λ of 1 s^{-2}. The parameters of the previous simulation are used again, leading to the results reported in Figs. 8–10.

Figure 8 shows that kinetic energy feedback eliminates the secular decay of rotor speeds seen to result from flywheel rotor damping in Fig. 6. The flywheel motor torques are shown in Fig. 9. It is immediately clear that the magnitudes do not increase with time as they do in Fig. 7. The power error e_p shown in the middle plot of Fig. 10 is quite small and leads to the kinetic energy error e_k displayed in the lower plot, which is small and periodic, in contrast to the secular decay obtained

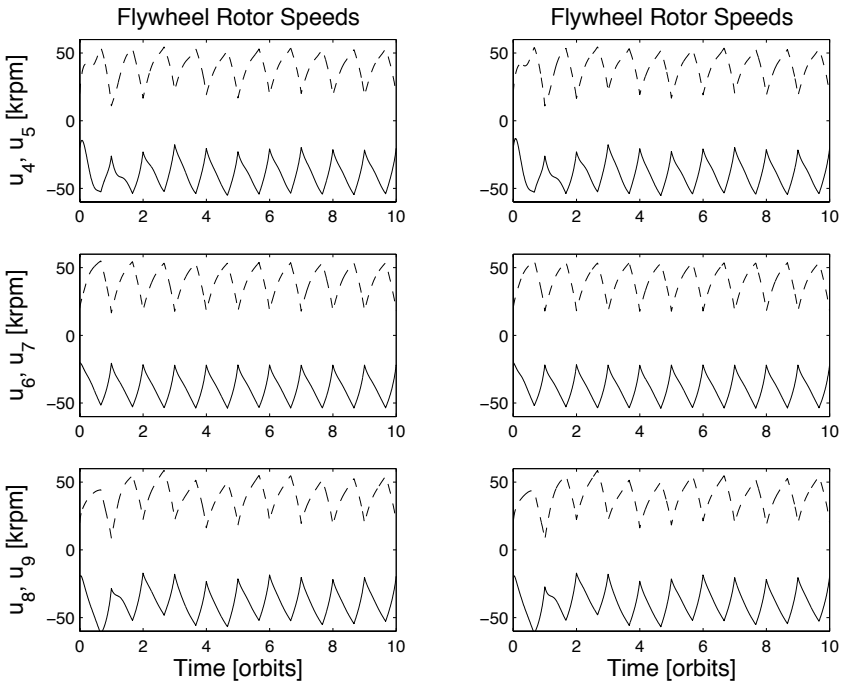

Figure 8: Flywheel Angular Speeds with Damped Flywheel Rotors and Kinetic Energy Error Feedback (Pseudo-Inverse left, Divided Power right)

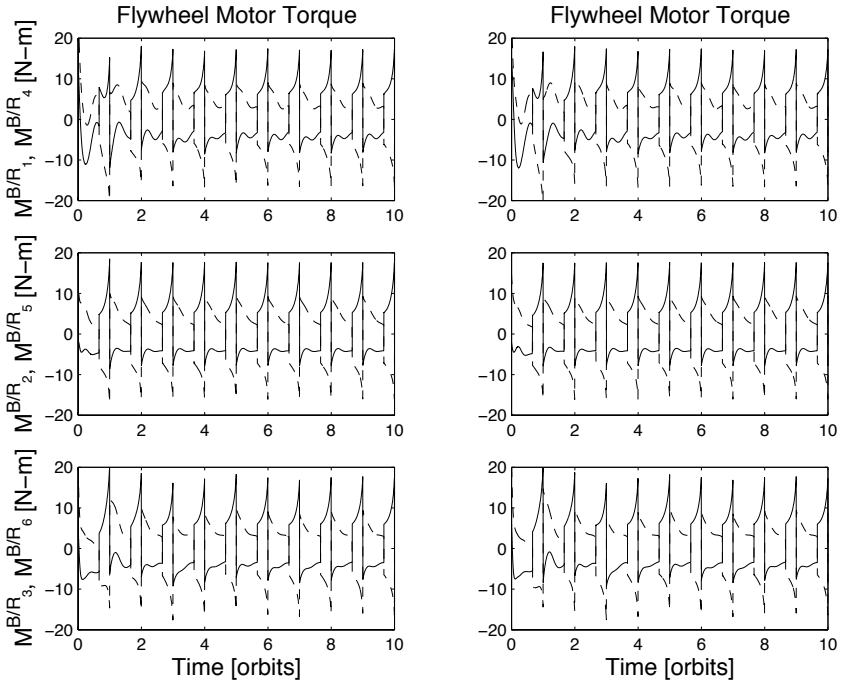

Figure 9: Flywheel Motor Torques with Damped Flywheel Rotors and Kinetic Energy Error Feedback (Pseudo-Inverse left, Divided Power right)

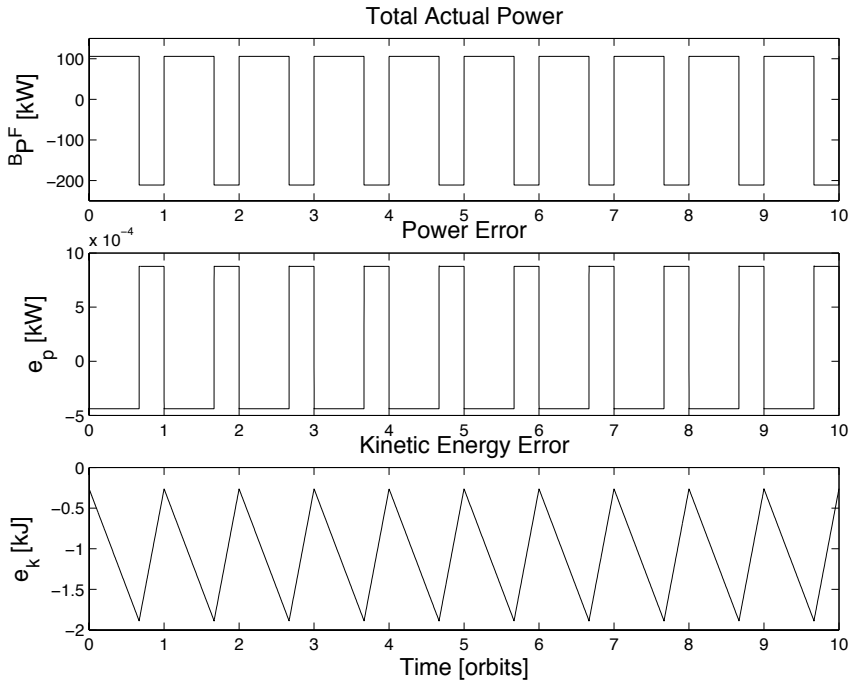

Figure 10: Power, Power Error, and Kinetic Energy Error with Damped Flywheel Rotors and Kinetic Energy Error Feedback

without energy feedback ($\lambda = 0$ s^{-2}).

The kinetic energy error feedback method compensates for damping very effectively, as illustrated by Figs. 8–10; these results are virtually the same as those obtained with $C_d = 0$ and no energy feedback, although space limitation prevent us from including them separately.

CONCLUSION

General, nonlinear equations governing motion of a rigid spacecraft containing flywheels and CMGs are presented in vector-dyadic form. A set of twelve scalar equations is obtained by applying the generic relationships to the special case of a complex gyrostat with three pairs of flywheels mounted in orthogonal directions. Existing literature contains equations for describing motion of a spacecraft with CMGs; they follow from the generic ones under two reasonable assumptions. The exact equations for the complex gyrostat, and the approximate relationships associated with CMGs are combined to form approximate equations for a spacecraft with flywheels and CMGs, and subsequently linearized and nondimensionalized in preparation for design of linear control laws.

A control law has been designed for an Earth-pointing spacecraft, and numerical simulation shows that it performs well in controlling torque equilibrium attitude, the energy stored in counter-rotating flywheels, and angular momentum of the flywheels and CMGs. Two steering laws are developed for ensuring that attitude control and energy storage requirements are met simultaneously by the flywheels. The design of a method for feeding back error in the rotational kinetic energy of the flywheel rotors in order to eliminate problems caused by rotor damping is shown to be effective.

One topic of future research that may be valuable is the study of controller performance in the face of imperfect knowledge of spacecraft inertia properties, or flywheel rotor pairs whose axial moments of inertia are not identical. Inclusion of a pre-filter would allow the control laws to estimate

these parameters from attitude response, and compensate for any significant changes in the mass distribution of the spacecraft over time. Another topic with possible merit is exploration of the best way to apportion the control torque between the flywheels and CMGs; an adaptive feature for distributing the workload unequally could be preferable to the practice of sharing it equally. Future spacecraft are likely to rely solely on flywheels, rather than a mixture of flywheels and CMGs, and the control laws developed here are easily applied to this special case.

The promising results demonstrated here for control of power, momentum, and attitude of Earth-pointing spacecraft suggest that it would be worthwhile to examine the very important class of inertially oriented spacecraft.

ACKNOWLEDGMENT

The research described herein was conducted as part of the Langley Research Center Creativity and Innovation initiative, and the authors are sincerely appreciative of all the support we received. A more detailed report of this work, which includes additional control law designs and simulation results, is available in Ref. [21]. The first author is especially grateful to the management of the Aerospace Systems Concepts and Analysis Competency, and the Spacecraft and Sensors Branch for their encouragement. Special thanks are due to Anne Costa for creating the illustrations that appear in Figs. 1 and 2.

REFERENCES

[1] Christopher, D. A., and Beach, R., "Flywheel Technology Development Program for Aerospace Applications," *IEEE Aerospace and Electronic Systems Magazine*, Vol. 13, Issue 6, June, 1998, pp. 9–14.

[2] Roithmayr, C. M., "International Space Station Attitude Motion Associated With Flywheel Energy Storage," *Proceedings of the Space Technology and Applications International Forum*, Albuquerque, NM, Jan. 30–Feb. 3, 2000, pp. 454–459.

[3] Wie, B., et al., "New Approach to Attitude/Momentum Control for the Space Station," *Journal of Guidance Control, and Dynamics*, Vol. 12, No. 5, 1989, pp. 714–722.

[4] Harduvel, J. T., "Continuous Momentum Management of Earth-Oriented Spacecraft," *Journal of Guidance Control, and Dynamics*, Vol. 15, No. 6, 1992, pp. 1417–1426.

[5] Kennel, H. F., *Steering Law for Parallel Mounted Double-Gimbaled Control Moment Gyros—Revision A*, NASA TM-82390, Jan. 1981.

[6] Notti, J. E., Cormack, A., and Klein, W. J., "Integrated Power/Attitude Control System (IPACS)," AIAA Paper No. 74-921, Mechanics and Control of Flight Conference, Anaheim, CA, Aug. 5–9, 1974.

[7] Hall, C. D., "High Speed Flywheels for Integrated Energy Storage and Attitude Control," *Proceedings of the 1997 American Control Conference*, Albuquerque, NM, June 4–6, 1997, Vol. 3, pp. 1894–1898.

[8] Tsiotras, P., Shen, H., and Hall, C. D., "Satellite Attitude Control and Power Tracking with Energy/Momentum Wheels," *Journal of Guidance Control, and Dynamics*, Vol. 24, No. 1, 2001, pp. 23–34.

[9] Costic, B. T., et al., "Energy Management and Attitude Control Strategies using Flywheels," *Proceedings of the 40th IEEE Conference on Decision and Control*, Orlando, FL, December 2001.

[10] Fausz, J. L., and Richie, D. J., "Flywheel Simultaneous Attitude Control and Energy Storage Using a VSCMG Configuration," *Proceedings of the 2000 IEEE International Conference on Control Applications*, Anchorage, AK, Sept. 2000, pp. 991–995.

[11] Richie, D. J., Tsiotras, P., and Fausz, J. L., "Simultaneous Attitude Control and Energy Storage Using VSCMGs— Theory and Simulation," *Proceedings of the 2001 American Control Conference*, Arlington, VA, June 25–27, 2001, Vol. 5, pp. 3973–3979.

[12] Yoon, H., and Tsiotras, P., "Spacecraft Adaptive Attitude and Power Tracking with Variable Speed Control Moment Gyroscopes," *Journal of Guidance, Control and Dynamics*, Vol. 25, No. 6, 2002, pp. 1081–1090.

[13] Varatharajoo, R., and Fasoulas, S., "Methodology for the Development of Combined Energy and Attitude Control Systems for Satellites," *Aerospace Science and Technology*, Vol. 6, No. 4, 2002, pp. 303–311.

[14] Kane, T. R., and Levinson, D. A., *Dynamics: Theory and Applications*, McGraw-Hill, New York, 1985.

[15] Mitiguy, P. C., and Reckdahl, K. J., "Efficient Dynamical Equations for Gyrostats," *Journal of Guidance, Control, and Dynamics*, Vol. 24, No. 6, 2001, pp. 1144–1156.

[16] Rheinfurth, M. H., and Carroll, S. N., *Space Station Rotational Equations of Motion*, NASA Technical Paper 2511, Marshall Space Flight Center, 1985.

[17] Kane, T. R., Likins, P. W., and Levinson, D. A., *Spacecraft Dynamics*, McGraw-Hill, New York, 1983.

[18] Roithmayr, C. M., *International Space Station Attitude Control and Energy Storage Experiment: Effects of Flywheel Torque*, NASA TM-1999-209100, NASA Langley Research Center, Hampton, VA, February, 1999.

[19] Lay, D. C., *Linear Algebra and its Applications*, Addison-Wesley, Reading, MA, 1994.

[20] Bryson, A. E., and Ho, Y-C., *Applied Optimal Control*, Hemisphere Publishing Corporation, New York, NY, 1975.

[21] Roithmayr, C. M., et al., *Dynamics and Control of Attitude, Power, and Momentum for a Spacecraft using Flywheels and Control Moment Gyroscopes*, to be published as a NASA TP.